Progress In Electromagnetics Research C, Vol. 127, 61–70, 2022

A Novel Balanced-to-Balanced Differential-Mode Negative Group Delay Microwave Circuit with Excellent Common-Mode Suppression

Zhongbao Wang*, Peng Han, Qi Chen, Hongmei Liu, and Shaojun Fang

Abstract—A novel balanced-to-balanced differential-mode negative group delay (NGD) microwave circuit with excellent common-mode suppression is proposed. The proposed circuit consists of two sections of coupled lines, six transmission lines, and four open-circuited stubs. The coupled lines combined with the open-circuited stubs produce the NGD characteristic, which is connected by the $\lambda/2$ transmission lines to form a balanced structure for excellent common-mode suppression. To verify the proposed balanced circuit, a microstrip circuit prototype with a center frequency of $f_0 = 1.0$ GHz is designed, fabricated, and measured. When the prototype is excited in differential mode, the measured NGD time at f_0 is -3.45 ns with an NGD bandwidth of 16.6 MHz (991.7–1008.3 MHz), insertion loss of less than 2.88 dB, and return loss of more than 11.7 dB. Furthermore, the measured common-mode suppression is greater than 41 dB in the NGD band.

1. INTRODUCTION

When developing today's increasingly complex microwave circuits and systems, engineers must contend with two issues: common-mode noise and signal crosstalk [1]. Balanced circuits can offer considerable immunity to environmental noise and broadband common-mode suppression (CMS) capability in comparison to conventional single-ended circuits [2]. Therefore, balanced microwave devices, such as the balanced power divider [3], balanced duplexer [4], and balanced coupler [5], have been widely adopted. Furthermore, because positive group delay (PGD) causes long delays and signal distortion, high-quality signal transmission demands attention to both anti-interference capabilities and signal phase characteristics. Negative group delay (NGD) circuits [6–10] are a useful technique to compensate for PGD and diminish the passband group delay's fluctuation [11]. And NGD circuits have improved feedforward amplifier efficiency [12], produced NGD characteristics in power dividers [13] and couplers [14] to minimize the effect of the PGD of traditional circuits, eliminated phase variation with frequency in broadband constant phase shifters [15], etc. Nevertheless, to the authors' knowledge, only a small portion of the noteworthy work completed so far is on balanced NGD microwave circuit [16–19].

Recently, a balanced-to-unbalanced (BTU) NGD power divider has been proposed [16]. However, the CMS of this BTU power divider is sacrificed in order to achieve the NGD feature, which has a weak common mode to single-ended suppression of less than 15 dB. Compared with [16], the CMS of the BTU NGD power divider has been improved in [17]. However, it must contend with the issues of high insertion loss (IL) and poor isolation. In response to the demands for fully-balanced system application, two balanced-to-balanced circuits integrated with differential-mode NGD properties have been proposed in [18, 19]. The additional lumped resistors needed for generating NGD and lower CMS of this circuit [18] indicate that there is more space for improvement. The transmission lines used in [19] are incompatible with commonly-used microstrip lines due to the design reliance on double-sided parallel strip lines. Therefore, it is required to provide a fully balanced NGD microwave circuit with a

Received 29 September 2022, Accepted 17 November 2022, Scheduled 28 November 2022
* Corresponding author: Zhongbao Wang (wangzb@dlmu.edu.cn).
The authors are with the School of Information Science and Technology, Dalian Maritime University, Dalian, Liaoning 116026, China.

fully distributed microstrip structure since this type of structure has the advantages of flexible design and simple manufacture.

In this paper, a novel balanced-to-balanced (BTB) differential-mode NGD microwave circuit, using a fully distributed structure, is proposed. The benefits of a simple microstrip structure, an excellent CMS, and a good NGD effect are all combined in this design. The theoretical derivation of the scattering matrix is carried out on the circuit topology. The parameter analysis and experimental results of the circuit design are given.

2. CIRCUIT TOPOLOGY AND THEORY ANALYSIS

Figure 1 depicts the schematic diagram of the proposed BTB NGD circuit, which has two balanced ports, A and B. The balanced port A is composed of ports 1 and 3, and the balanced port B of ports 2 and 4. This structure contains four transmission lines with an electrical length of θ, four open-circuited stubs with an electrical length of $\pi/4$, and two transmission lines with an electrical length of π, and the above characteristic impedances are all Z_0. This structure also includes two coupled lines with an electrical length of $\pi/2$. The even- and odd-mode characteristic impedances of the coupled lines satisfy (1).

$$Z_0^2 = Z_{0e}Z_{0o} \tag{1}$$

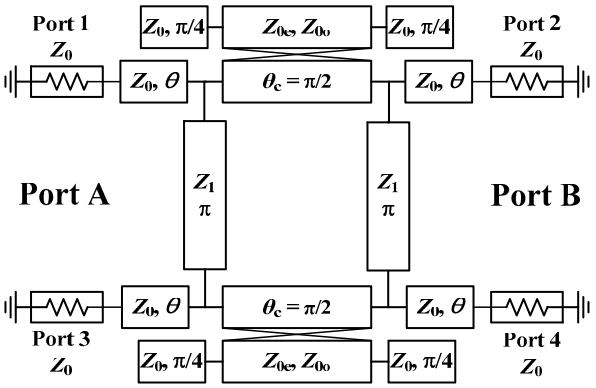

Figure 1. Schematic of the proposed BTB NGD microwave circuit.

The scattering parameters for the mixed mode under Figure 1's topology are provided in (2).

$$\begin{cases} S_{\mathrm{ddAA}} = \dfrac{(S_{11} + S_{33} - S_{13} - S_{31})}{2} \\ S_{\mathrm{ddBA}} = \dfrac{(S_{21} - S_{23} + S_{43} - S_{41})}{2} \\ S_{\mathrm{ccAA}} = \dfrac{(S_{11} + S_{33} + S_{13} + S_{31})}{2} \\ S_{\mathrm{ccBA}} = \dfrac{(S_{21} + S_{23} + S_{43} + S_{41})}{2} \end{cases} \tag{2}$$

The proposed BTB NGD circuit is horizontally symmetric, which can be rigorously analyzed using the even- and odd-mode method. As indicated in Figure 2, the circuit can be divided into two two-port networks. The mixed scattering parameters of the balanced topology, as shown in Figure 1, and the scattering parameters of the two-port topology, obtained using the odd-even mode analysis method, as shown in Figure 2, have the following relationship (3).

$$\begin{cases} S_{\mathrm{ddAA}} = S_{11o} \\ S_{\mathrm{ddBA}} = S_{21o} \\ S_{\mathrm{ccAA}} = S_{11e} \\ S_{\mathrm{ccBA}} = S_{21e} \end{cases} \tag{3}$$

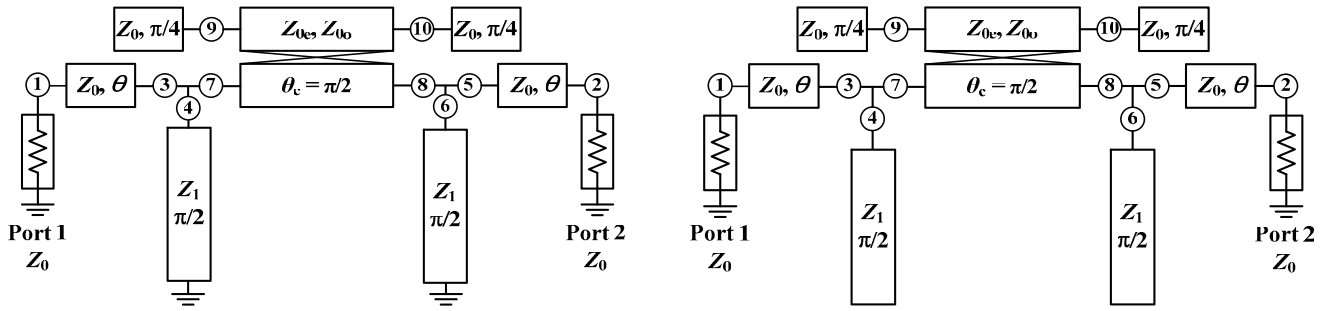

Figure 2. Even- and odd-mode sub-circuits of the proposed BTB NGD microwave circuit. (a) Odd-mode, (b) even-mode.

where S_{11o} and S_{21o} represent the reflection and transmission coefficients of the odd-mode topology, respectively. S_{11e} and S_{21e} represent the reflection and transmission coefficients of the even-mode topology, respectively.

According to (3), the differential-mode group delay is related to the scattering parameter S_{21o}. Considering that the derivation processes of the odd-mode topology and even-mode topology are the same, the following only derives the scattering parameter of the odd-mode topology and does not repeat the derivation of the even-mode topology.

According to microwave theory, the S-parameter matrix of an ideal 90° coupler is expressed as

$$[S]_{CL} = \begin{bmatrix} 0 & -j\sqrt{1-k^2} & k & 0 \\ -j\sqrt{1-k^2} & 0 & 0 & k \\ k & 0 & 0 & -j\sqrt{1-k^2} \\ 0 & k & -j\sqrt{1-k^2} & 0 \end{bmatrix} \tag{4}$$

It is assumed that the open-circuited stub with an electrical length of $\pi/4$ and the short-circuited stub of $\pi/2$ are lossy. The loss is set to parameter a. The transmission lines with electrical length θ are lossless structures, including the delay effect with the following parameters.

$$\begin{cases} a_{\pi/2} = a_{\pi/4}^2 \\ x_{\pi/4} = e^{-j\omega\tau_1} \\ x_{\pi/2} = e^{-j\omega 2\tau_1} \\ x_\theta = e^{-j\omega\tau_2} \end{cases} \tag{5}$$

where τ_1 is the time delay of the transmission line with an electrical length of $\pi/4$, and τ_2 is the time delay of the transmission line with an electrical length of θ.

The input impedance of the open-circuited stub and short-circuited stub can be expressed as [8]

$$Z = \begin{cases} Z_0 \dfrac{1+a^2x^2}{1-a^2x^2} & \text{if } Z_L = \infty \\ Z_0 \dfrac{1-a^2x^2}{1+a^2x^2} & \text{if } Z_L = 0 \end{cases} \tag{6}$$

According to the circuit theory, the ideal S-parameter matrix at three ports (③④⑦, ⑤⑥⑧) is defined as

$$[S]_T = \begin{bmatrix} -\dfrac{1}{3} & \dfrac{2}{3} & \dfrac{2}{3} \\ \dfrac{2}{3} & -\dfrac{1}{3} & \dfrac{2}{3} \\ \dfrac{2}{3} & \dfrac{2}{3} & -\dfrac{1}{3} \end{bmatrix} \tag{7}$$

From (4)–(6), we can get the two-port S-parameter matrix of the coupled line part.

$$\begin{bmatrix} b_7 \\ b_8 \end{bmatrix} = \begin{bmatrix} S_{77} & S_{78} \\ S_{87} & S_{88} \end{bmatrix} \times \begin{bmatrix} a_7 \\ a_8 \end{bmatrix} \tag{8}$$

with

$$\begin{cases} S_{77} = \dfrac{a_{\pi/4}^2 x_{\pi/4}^2 \zeta^2}{1 + a_{\pi/4}^4 x_{\pi/4}^4 \zeta_0^2} \\ S_{87} = \dfrac{-j\zeta_0 \left(1 + a_{\pi/4}^4 x_{\pi/4}^4\right)}{1 + a_{\pi/4}^4 x_{\pi/4}^4 \zeta_0^2} \\ S_{77} = S_{88} \\ S_{87} = S_{78} \end{cases} \tag{9}$$

where $\zeta = k$, $\zeta_0 = \sqrt{1 - k^2}$.

From (5)–(7), we can get the two-port S-parameter matrix of the three-port part.

$$\begin{cases} \begin{bmatrix} b_3 \\ a_7 \end{bmatrix} = \begin{bmatrix} \dfrac{a_{\pi/2}^2 x_{\pi/2}^2 + 1}{a_{\pi/2}^2 x_{\pi/2}^2 - 3} & \dfrac{2a_{\pi/2}^2 x_{\pi/2}^2 - 2}{a_{\pi/2}^2 x_{\pi/2}^2 - 3} \\ \dfrac{2a_{\pi/2}^2 x_{\pi/2}^2 - 2}{a_{\pi/2}^2 x_{\pi/2}^2 - 3} & \dfrac{a_{\pi/2}^2 x_{\pi/2}^2 + 1}{a_{\pi/2}^2 x_{\pi/2}^2 - 3} \end{bmatrix} \times \begin{bmatrix} a_3 \\ b_7 \end{bmatrix} \\ \begin{bmatrix} b_5 \\ a_8 \end{bmatrix} = \begin{bmatrix} \dfrac{a_{\pi/2}^2 x_{\pi/2}^2 + 1}{a_{\pi/2}^2 x_{\pi/2}^2 - 3} & \dfrac{2a_{\pi/2}^2 x_{\pi/2}^2 - 2}{a_{\pi/2}^2 x_{\pi/2}^2 - 3} \\ \dfrac{2a_{\pi/2}^2 x_{\pi/2}^2 - 2}{a_{\pi/2}^2 x_{\pi/2}^2 - 3} & \dfrac{a_{\pi/2}^2 x_{\pi/2}^2 + 1}{a_{\pi/2}^2 x_{\pi/2}^2 - 3} \end{bmatrix} \times \begin{bmatrix} a_5 \\ b_8 \end{bmatrix} \end{cases} \tag{10}$$

The two-port S-parameter matrix of a lossless transmission line with an electrical length of θ is expressed as

$$\begin{cases} \begin{bmatrix} b_1 \\ a_3 \end{bmatrix} = \begin{bmatrix} 0 & x_\theta \\ x_\theta & 0 \end{bmatrix} \times \begin{bmatrix} a_1 \\ b_3 \end{bmatrix} \\ \begin{bmatrix} b_2 \\ a_5 \end{bmatrix} = \begin{bmatrix} 0 & x_\theta \\ x_\theta & 0 \end{bmatrix} \times \begin{bmatrix} a_2 \\ b_5 \end{bmatrix} \end{cases} \tag{11}$$

Combining (8)–(11), we can get the two-port S-parameter matrix of odd-mode topology as

$$\begin{cases} \begin{bmatrix} b_1 \\ b_2 \end{bmatrix} = \begin{bmatrix} S_{11} & S_{12} \\ S_{21} & S_{22} \end{bmatrix} \times \begin{bmatrix} a_1 \\ a_2 \end{bmatrix} \\ S_{11} = x_\theta^2 \dfrac{\left(g_4^2 - g_3^2\right)\left[g_3\left(g_2^2 - g_1^2\right) + g_1\right] - g_3^2 g_1 + g_3}{g_3^2\left(g_1^2 - g_2^2\right) - 2g_1 g_3 + 1} \\ S_{21} = x_\theta^2 \dfrac{g_2 g_4^2}{g_3^2\left(g_1^2 - g_2^2\right) - 2g_1 g_3 + 1} \\ S_{11} = S_{22}, \;\; S_{12} = S_{21} \end{cases} \tag{12}$$

with

$$\begin{cases} g_1 = \dfrac{a_{\pi/4}^2 x_{\pi/4}^2 \zeta^2}{1 + a_{\pi/4}^4 x_{\pi/4}^4 \zeta_0^2}, \quad g_2 = \dfrac{-j\zeta_0\left(1 + a_{\pi/4}^4 x_{\pi/4}^4\right)}{1 + a_{\pi/4}^4 x_{\pi/4}^4 \zeta_0^2} \\ g_3 = \dfrac{a_{\pi/4}^4 x_{\pi/4}^4 + 1}{a_{\pi/4}^4 x_{\pi/4}^4 - 3}, \qquad g_4 = \dfrac{2a_{\pi/4}^4 x_{\pi/4}^4 - 2}{a_{\pi/4}^4 x_{\pi/4}^4 - 3} \end{cases} \tag{13}$$

From (12) and (13), the modulus of S_{21} can be expressed as

$$|S_{21}(\omega)| = \sqrt{\frac{R_1^2(\omega) + I_1^2(\omega)}{R_2^2(\omega) + I_2^2(\omega)}} \tag{14}$$

with

$$\begin{cases} R_1 = -4\zeta_0 \sum\limits_{i_1=0}^{3} a^{4i_1} m_{i_1} \sin(4i_1\tau_1\omega + 2\tau_2\omega) \\ I_1 = -4\zeta_0 \sum\limits_{i_1=0}^{3} a^{4i_1} m_{i_1} \cos(4i_1\tau_1\omega + 2\tau_2\omega) \\ R_2 = \left(\begin{array}{l} 9 + \sum\limits_{i_2=1}^{6} p_{i_2} a^{2i_3} \cos(2i_2\tau_1\omega) + \\ \zeta_0^2 + \zeta_0^2 \sum\limits_{i_2=1}^{6} q_{i_2} a^{2i_3} \cos(2i_2\tau_1\omega) \end{array} \right) \\ I_2 = \left(\begin{array}{l} \sum\limits_{i_2=1}^{6} -p_{i_2} a^{2i_4} \sin(2i_2\tau_1\omega) + \\ \zeta_0^2 \sum\limits_{i_2=1}^{6} -q_{i_2} a^{2i_4} \sin(2i_2\tau_1\omega) \end{array} \right) \end{cases} \tag{15}$$

and

$$\begin{cases} m_0 = 1, m_1 = -1, m_2 = -1, m_3 = 1 \\ p_1 = 6, p_2 = -5, p_3 = 4, p_4 = 3, p_5 = -2, p_6 = 1 \\ q_1 = -6, q_2 = 11, q_3 = -4, q_4 = -5, q_5 = 2, q_6 = 1 \end{cases} \tag{16}$$

The transmission phase of the topology is expressed as $\varphi(\omega) = \text{ang}[S_{21}(\omega)]$, which can be derived from the transmission coefficient expression introduced in (12) and (13), and the detailed expression is expressed as

$$\varphi(\omega) = \varphi_1(\omega) - \varphi_2(\omega) \tag{17}$$

with

$$\begin{cases} \varphi_1(\omega) = \arctan \dfrac{I_1(\omega)}{R_1(\omega)} \\ \varphi_2(\omega) = \arctan \dfrac{I_2(\omega)}{R_2(\omega)} \end{cases} \tag{18}$$

According to the expression of the transmission phase, the definition of the expected group delay can be expressed by

$$\tau(\omega) = \frac{-\partial\varphi(\omega)}{\partial\omega} = \tau_2(\omega) - \tau_1(\omega) \tag{19}$$

with

$$\begin{cases} \tau_1(\omega) = -\dfrac{\partial\varphi_1(\omega)}{\partial\omega} \\ \tau_2(\omega) = -\dfrac{\partial\varphi_2(\omega)}{\partial\omega} \end{cases} \tag{20}$$

Combining the obtained (14)–(18), we can get the complete expression of group delay.

$$\tau(\omega) = \left(\begin{array}{l} \dfrac{I_2'(\omega) R_2(\omega) - I_2(\omega) R_2'(\omega)}{R_2^2(\omega) + I_2^2(\omega)} \\ -\dfrac{I_1'(\omega) R_1(\omega) - I_1(\omega) R_1'(\omega)}{R_1^2(\omega) + I_1^2(\omega)} \end{array} \right) \tag{21}$$

with

$$\begin{cases} R_1' = (-16i_1\tau_1 - 8\tau_2)\,\zeta_0 \sum\limits_{i_1=0}^{3} a^{4i_1} m_{i_1} \cos(4i_1\tau_1\omega + 2\tau_2\omega) \\ I_1' = (16i_1\tau_1 + 8\tau_2)\,\zeta_0 \sum\limits_{i_1=0}^{3} a^{4i_1} m_{i_1} \sin(4i_1\tau_1\omega + 2\tau_2\omega) \\ R_2' = \begin{pmatrix} -2i_2\tau_1 \sum\limits_{i_2=1}^{6} p_{i_2} a^{2i_3} \sin(2i_2\tau_1\omega) - \\ 2i_2\tau_1\zeta_0^2 \sum\limits_{i_2=1}^{6} q_{i_2} a^{2i_3} \sin(2i_2\tau_1\omega) \end{pmatrix} \\ I_2' = \begin{pmatrix} -2i_2\tau_1 \sum\limits_{i_2=1}^{6} p_{i_2} a^{2i_4} \cos(2i_2\tau_1\omega) - \\ 2i_2\tau_1\zeta_0^2 \sum\limits_{i_2=1}^{6} q_{i_2} a^{2i_4} \cos(2i_2\tau_1\omega) \end{pmatrix} \end{cases} \tag{22}$$

and

$$\begin{cases} m_0 = 1, m_1 = -1, m_2 = -1, m_3 = 1 \\ p_1 = 6, p_2 = -5, p_3 = 4, p_4 = 3, p_5 = -2, p_6 = 1 \\ q_1 = -6, q_2 = 11, q_3 = -4, q_4 = -5, q_5 = 2, q_6 = 1 \end{cases} \tag{23}$$

Based on the above analysis, a circuit is designed in order to verify the proposed BTB NGD circuit. Parameter analysis, simulation, and test results will be introduced in the next section.

3. PARAMETER ANALYSIS AND EXPERIMENTAL VERIFICATION

Through the analysis in Section 2, in the differential-mode (i.e., odd-mode) topology, the half-wavelength transmission line is equivalent to a quarter-wavelength short-circuited transmission line, so the proposed circuit achieves differential-mode transmission. In the common-mode (i.e., even-mode) topology, the half-wavelength transmission line is equivalent to a quarter-wavelength open-circuited transmission line; therefore, the proposed circuit achieves common-mode rejection. Based on the above analysis, the following will analyze the influence of the characteristic impedance of the half-wavelength transmission line on the common-mode suppression. Besides, the coupled line part is used to generate NGD characteristics, so a parametric analysis will also be performed on the coupling level and the electrical length of the coupled lines.

The first thing to analyze is the influence of the characteristic impedance Z_1 of the half-wavelength transmission line on the proposed BTB NGD circuit. As can be seen from Figure 3, the characteristic impedance Z_1 chiefly affects the CMS bandwidth. When the characteristic impedance Z_1 decreases from 75 to 25 Ω, the bandwidth for 30-dB CMS (i.e., $|S_{\mathrm{ccBA}}| < -30$ dB) increases, and the differential-mode NGD at the center frequency f_0 of 1.0 GHz increases from -4.659 to -4.331 ns. At the same time, the differential-mode return loss (or $|S_{\mathrm{ddAA}}|$) at f_0 has no change.

Figure 4 gives the effect of the coupling level k of the coupled lines on the performances of the proposed BTB NGD circuit. With the change of the coupling level of the coupled lines, the CMS ($|S_{\mathrm{ccBA}}|$) remains unchanged. When the coupling level increases from -19 to -17 dB, the differential-mode NGD at the center frequency changes from -3.303 to -4.912 ns with $|S_{\mathrm{ddAA}}|$ increased from -14.2 to -11.1 dB and $|S_{\mathrm{ddBA}}|$ decreased from -2.0 to -3.0 dB. Thus, there is a trade-off among the differential-mode NGD, return loss, and insertion loss.

The effect of electrical length θ_c of the coupled lines on the proposed BTB NGD circuit is introduced in Figure 5. When the electrical length θ_c increases from 80° to 100°, the NGD center frequency falls from 1.059 to 0.947 GHz with minor changes of differential-mode NGD, return loss, and insertion loss

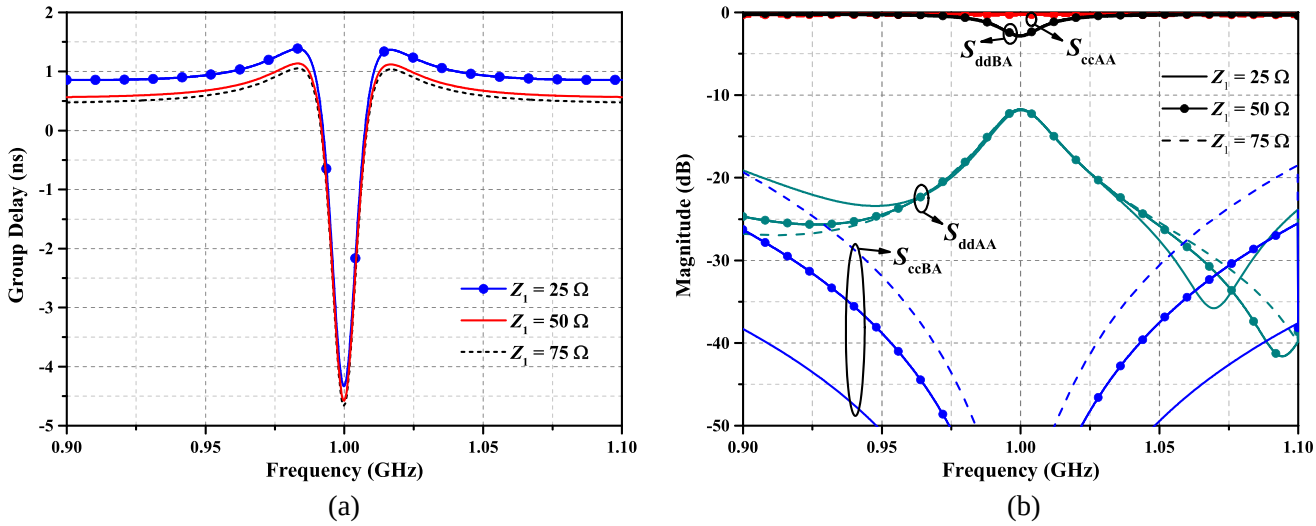

Figure 3. Effect of Z_1 on the performances of the proposed BTB NGD microwave circuit. (a) Differential-mode group delay. (b) Mixed-mode S-parameters.

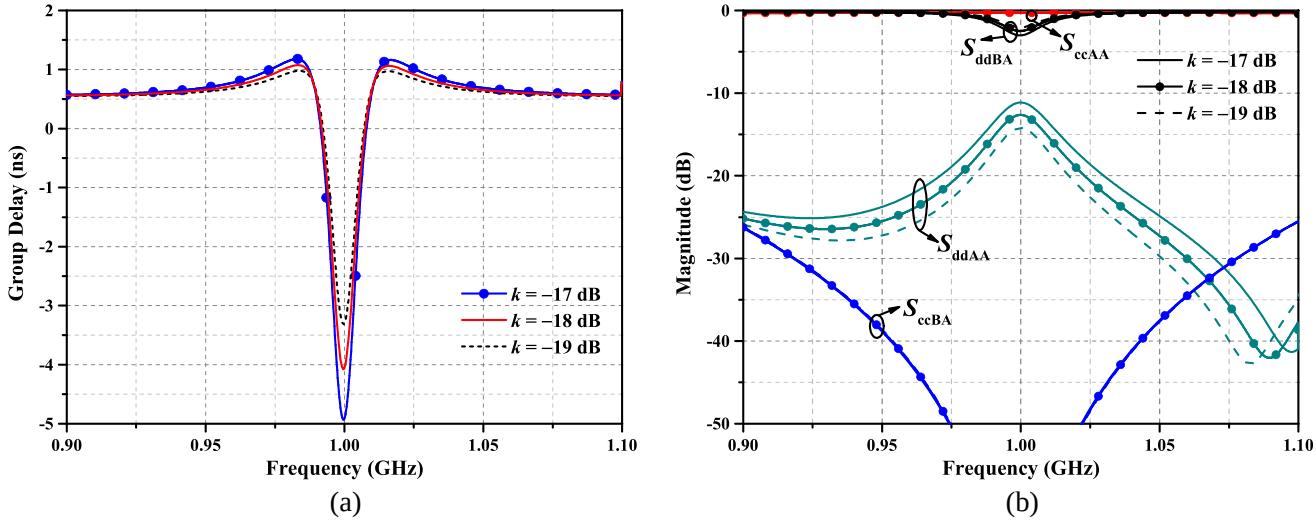

Figure 4. Effect of k on the performances of the proposed BTB NGD microwave circuit. (a) Differential-mode group delay. (b) Mixed-mode S-parameters.

at NGD center frequency. Also, the electrical length θ_c of the coupled lines has a negligible effect on the CMS.

In order to experimentally demonstrate the previous theory and analysis, a BTB NGD microstrip circuit with a center frequency f_0 of 1.0 GHz is designed. The circuit is implemented on an FR4 substrate (relative permittivity $\varepsilon_r = 4.4$, thickness $h = 1.5$ mm, and dielectric loss tangent $\tan\delta = 0.02$). The optimal dimensions must consider the discontinuous interface, dielectric loss, and the limited metal conductivity of the microstrip lines. Therefore, the final dimensions are obtained through HFSS electromagnetic simulation and are given in Table 1. The circuit prototype is shown in Figure 6. The overall size is $0.43\lambda_g \times 0.58\lambda_g$.

Figure 7 gives simulated and measured group delays and mixed-mode S-parameters of the proposed BTB NGD circuit. At the center frequency of $f_0 = 1.0$ GHz, the measured differential-mode NGD time is -3.45 ns. The fractional bandwidth (FBW) for differential-mode group delay less than 0 ns is 1.66% (0.9917–1.0083 GHz). As shown in Figure 6(b), the measured insertion loss of the common mode (i.e.,

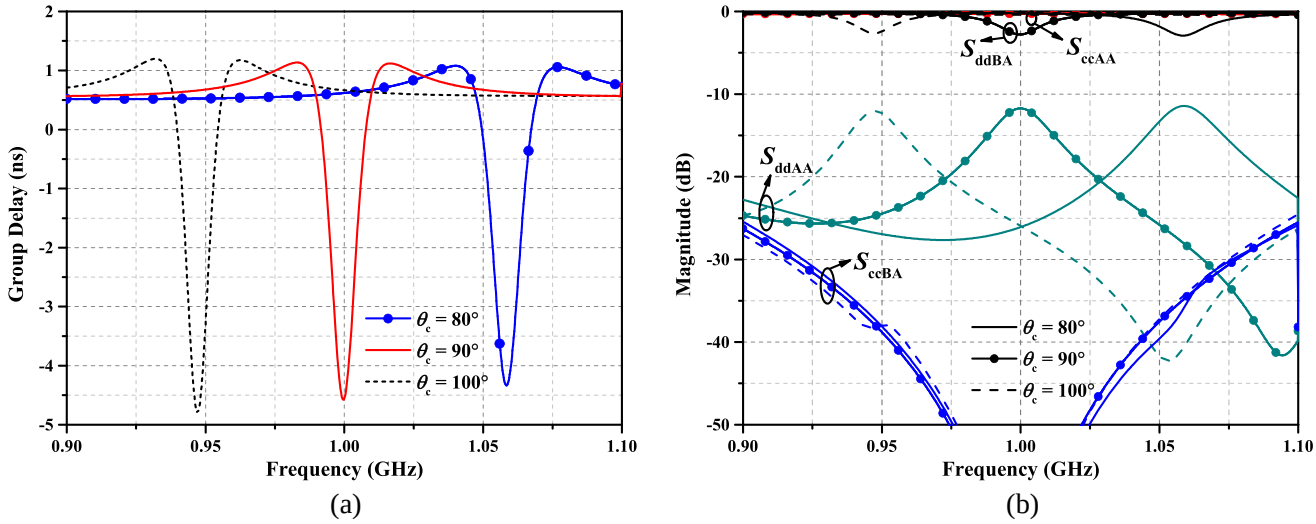

Figure 5. Effect of θ_c on the performances of the proposed BTB NGD microwave circuit. (a) Differential-mode group delay. (b) Mixed-mode S-parameters.

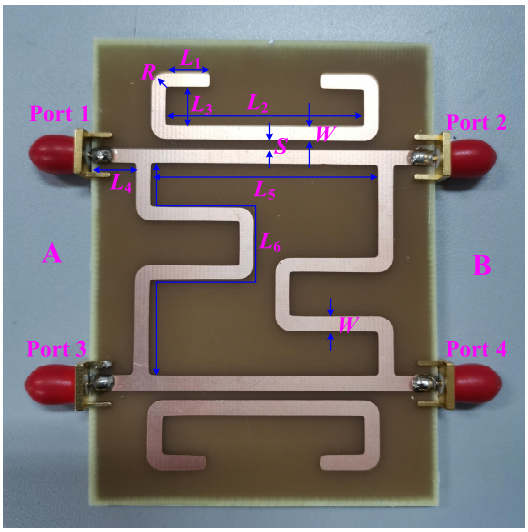

Figure 6. Photograph of the proposed BTB NGD microwave circuit.

CMS) reaches 41 dB at the NGD center frequency. From 0.9 to 1.1 GHz, the CMS is larger than 21 dB. The measured return loss of the differential mode is better than 11.7 dB, and the insertion loss is better than 2.88 dB in the NGD band. There is an acceptable difference between the measured and simulated results, mainly due to the welding deviation of SMA connector and discontinuous interfaces in the layout.

Usually, the NGD circuit is evaluated using the figure of merit (FOM) [17], which is defined as

$$\mathrm{FOM} = |\mathrm{NGD}(f_0)| \times \mathrm{BW}_{\mathrm{NGD}} \times |S_{\mathrm{ddBA}}(f_0)| \tag{24}$$

Table 1. Dimensions of the proposed BTB NGD microwave circuit (unit: mm).

W	S	R	L_1	L_2	L_3	L_4	L_5	L_6
2.85	2.1	2.85	9.0	40.4	8.0	9.1	46.1	82.1

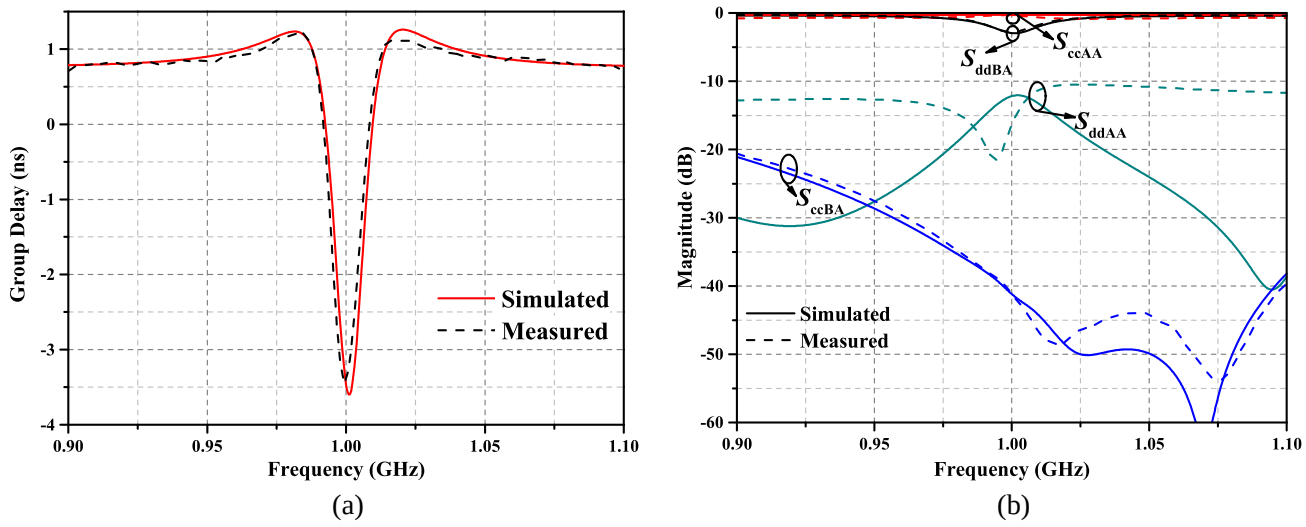

Figure 7. Simulation and measurement results of the proposed BTB NGD microwave circuit. (a) Differential-mode group delay. (b) Mixed-mode scattering parameter.

Table 2. Comparison with previous balanced NGD microwave circuits.

Reference	f_0 (GHz)	NGD (ns)	IL (dB)	RL (dB)	CMS (dB)	NGD-FBW (%)	FOM	Size ($\lambda_g \times \lambda_g$)	Use of resistor	Type
[16]	1.8	−1.10	5.4	15.0	15.0	1.9	0.021	0.55×0.25	Yes	BTU
[17]	1.0	−2.06	7.8	25.7	37.3	4.0	0.034	0.57×0.30	Yes	BTU
[18]	1.0	−0.22	3.7	10.0	18.0	8.8	0.013	-	Yes	BTB
[19]	1.227	−1.60	2.49	14.5	30.8	1.47	0.022	0.41×0.30	No	BTB
	1.575	−1.43	3.55	13.3		1.46	0.022			
This work	1.0	−3.45	2.88	11.7	41.0	1.66	0.041	0.43×0.58	No	BTB

Comparisons with previous balanced NGD circuits are given in Table 2. Compared with [16–19], the proposed BTB NGD circuit has excellent common-mode suppression and large FOM.

4. CONCLUSION

In this paper, a BTB NGD circuit with excellent common-mode suppression has been presented. The coupled lines combined with the open-circuited stubs have been used to realize the NGD characteristic, which is connected by the $\lambda/2$ transmission lines to form a fully-balanced structure for excellent CMS. The mixed-mode scattering parameter and group delay have been derived. A 1.0-GHz prototype with an NGD time of −3.45 ns has been designed, fabricated, and measured. The proposed BTB NGD microwave circuit has larger CMS and FOM than the previous balanced NGD circuits. In addition, the proposed fully-distributed circuit topology does not need any additional lumped elements and therefore is very suitable for high-frequency/microwave balanced circuits and systems. It will shine in NGD-based compensation technology [11, 12].

ACKNOWLEDGMENT

This work was supported by the National Natural Science Foundation of China (No. 61871417), the Liaoning Revitalization Talents Program (No. XLYC2007024), the Natural Science Foundation of Liaoning Province (No. 2020-MS-127), and the Fundamental Research Funds for the Central Universities (No. 3132022243).

REFERENCES

1. Feng, W., W. Che, and Q. Xue, "New balance — Applications for dual-mode ring resonators in planar balanced circuits," *IEEE Microw. Mag.*, Vol. 20, No. 7, 15–23, Jul. 2019.
2. Zhang, Y., Y. Wu, Y. Wei, and W. Wang, "Novel planar balanced bandpass filter with wideband common-mode suppression and in-band common-mode noise absorption," *Int. J. RF Microw. Comput. Aided Eng.*, Vol. 31, No. 1, e22483, Jan. 2021.
3. Shi, J., K. Xu, W. Zhang, J. Chen, and G. Zhai, "An approach to 1-to-2N way microstrip balanced power divider," *IEEE Trans. Microw. Theory Tech.*, Vol. 64, No. 12, 4222–4231, Dec. 2016.
4. Fernández-Prieto, A., A. Lujambio, F. Martín, J. Martel, F. Medina, and R. R. Boix, "Compact balanced-to-balanced diplexer based on split-ring resonators balanced bandpass filters," *IEEE Microw. Wireless Compon. Lett.*, Vol. 28, No. 3, 218–220, Mar. 2018.
5. Jiao, L., Y. Wu, W. Zhang, M. Li, Y. Liu, Q. Xue, and Z. Ghassemlooy, "Design methodology for six-port equal/unequal quadrature and rat-race couplers with balanced and unbalanced ports terminated by arbitrary resistances," *IEEE Trans. Microw. Theory Tech.*, Vol. 66, No. 3, 1249–1262, Mar. 2018.
6. Ravelo, B., "Theory of coupled line coupler-based negative group delay microwave circuit," *IEEE Trans. Microw. Theory Techn.*, Vol. 64, No. 11, 3604–3611, Nov. 2016.
7. Chaudhary, G. and Y. Jeong, "Negative group delay phenomenon analysis using finite unloaded quality factor resonators," *Progress In Electromagnetics Research*, Vol. 156, 55–62, 2016.
8. Ravelo, B., N. Li, F. Wan, and J. Feng, "Design, modeling and synthesis of negative group delay IL-shape topology," *IEEE Access*, Vol. 7, 153900–153909, 2019.
9. Wan, F., N. Li, B. Ravelo, and J. Ge, "O=O shape low-loss negative group delay microstrip circuit," *IEEE Trans. Circuits Syst. II, Exp. Briefs*, Vol. 67, No. 10, 1795–1799, Oct. 2020.
10. Wan, F., N. Li, B. Ravelo, W. Rahajandraibe, and S. Lalléchère, "Design of _I_ shape stub-based negative group delay circuit," *IEEE Des. Test*, Vol. 38, No. 2, 78–88, Apr. 2021.
11. Shao, T., Z. Wang, S. Fang, Y. Liu, and Z. Chen, "A full-passband linear-phase band-pass filter equalized with negative group delay circuits," *IEEE Access*, Vol. 8, 43336–43343, 2020.
12. Choi, H., Y. Jeong, C. D. Kim, and J. S. Kenney, "Efficiency enhancement of feedforward amplifiers by employing a negative group-delay circuit," *IEEE Trans. Microw. Theory Techn.*, Vol. 58, No. 5, 1116–1125, May 2010.
13. Chaudhary, G. and Y. Jeong, "Negative group delay phenomenon analysis in power divider: Coupling matrix approach," *IEEE Trans. Compon. Pack. Manuf. Technol.*, Vol. 7, No. 9, 1543–1551, Sept. 2017.
14. Wu, Y., H. Wang, Z. Zhuang, Y. Liu, Q. Xue, and A. A. Kishk, "A novel arbitrary terminated unequal coupler with bandwidth-enhanced positive and negative group delay characteristics," *IEEE Trans. Microw. Theory Techn.*, Vol. 66, No. 5, 2170–2184, May 2018.
15. Ravelo, B., M. Le Roy, and A. Perennec, "Application of negative group delay active circuits to the design of broadband and constant phase shifters," *Microw. Opt. Technol. Lett.*, Vol. 50, No. 12, 3078–3080, Dec. 2008.
16. Shi, J., Z. Chen, and K. Xu, "Negative group delay power dividing network with balanced-to-single-ended topology," *IET Microw. Antennas Propag.*, Vol. 13, No. 10, 1705–1710, Aug. 2019.
17. Zhu, Z., Z. Wang, S. Zhao, H. Liu, and S. Fang, "A novel balanced-to-unbalanced negative group delay power divider with good common-mode suppression," *Int. J. RF Microw. Comput. Aided Eng.*, Vol. 32, No. 7, e23173, Jul. 2022.
18. Zhu, Z., Z. Wang, Y. Meng, S. Fang, and H. Liu, "Balanced microstrip circuit with differential negative group delay characteristics," *Cross Strait Radio Science and Wireless Technology Conference*, 257–259, Oct. 2021.
19. Wang, Z. S. Zhao, H. Liu, and S. Fang, "A compact dual-band differential negative group delay circuit with wideband common mode suppression," *IEEE J. Microw.*, Vol. 2, No. 4, 720–725, 2022.